

Integrated photonic refractive index sensors

Master thesis

Lennart Wevers

June 26, 2015

Applied Physics

LioniX

Laser Physics and Nonlinear Optics

University Twente

Msc. graduation committee

Prof. Dr. K.J. Boller

Ir. F. Schreuder

Prof. Dr. J.L. Herek

Dr. P.J.M. van der Slot

CONTENTS

1	INTRODUCTION	5
1.1	General introduction	5
1.2	Outline	6
2	THEORY OF INTEGRATED PHOTONIC REFRACTIVE INDEX SENSORS	7
2.1	Refractive index sensor	7
2.2	introduction to Mach-Zehnder interferometer	8
2.3	Theory of the Mach-Zehnder interferometer	9
2.4	MZI theoretical performance	11
2.5	Introduction to microring resonator	13
2.6	Theory of the microring resonator	13
3	SIGNAL PROCESSING	17
3.1	Fourier transform	17
3.2	Least Squared Error fit	19
3.3	Error analyses for noise	20
4	USABILITY OF MZI AND MRR	23
4.1	MZI comparison based on theory	23
4.2	Measurement setup	24
4.3	VCSEL calibration	26
4.4	Comparison based on experimental measurements	26
5	MULTIPATH INTERFEROMETER	29
5.1	theory of the multipath interferometer	29
5.2	measurements	31
5.3	Sensing window refractive index change	31
5.4	Temperature change	33
5.5	Conclusion	34
6	MORE ADVANCED USE MICRORING RESONATOR	35
6.1	Absorption sensor	35

INTRODUCTION

1.1 GENERAL INTRODUCTION

Refractive index is a material property describing the linear response of a medium to an applied EM field (typically an optical wave) and equals to the ratio of the phase velocity of light in vacuum to that in the medium. The refractive index of a material is dependent on the material, temperature, pressure and stress. This allows translating a change in refractive index into one of these other properties. Therefore, by measuring the change in refractive index, a change in one of these properties can be measured as long as the remaining properties are kept constant. A device that measures the refractive index is called a refractive index sensor.

Many different refractive index sensor exists, varying in both size and the method of detection. In this work we focus on integrated optical sensors. On such a device multiple photonic functions are integrated on a single optical chip. Compared to other fields of optics, this allows for cheap, small and stable devices. These chips consist of a planar high refractive index material with the desired structure, called core. This core is surround by a lower refractive index material, called cladding. Light propagating through this chip is guided by the core, however the propagating light wave is not completely confined within this core. This means that this light is affected by both the refractive indexes of the core and cladding, resulting in an effective refractive index with a value between that of the core and cladding. For a refractive index sensor this effect is used to guide a light wave through the to be measured medium of interest, by locally removing the cladding and replacing it for this medium of interest, which can be a gas, liquid or solid.

In this thesis we compare the difference between the microring resonator (MRR) and the Mach-Zehnder interferometer (MZI). For a fixed wavelength the transmission of both these sensors dependents mainly on the effective refractive index. The comparison between these sensors is done to determine which has the lowest measurable change in refractive index (sensitivity). With the knowledge from these sensors two more advanced applications are discussed, which includes a MRR used to measure absorption and a multipath interferometer refractive index sensor that allows for multiplexing refractive index sensors. One advantage of all these sensors is that their data can be processed with a single algorithm, the Least Square Error fit (LSE), which is in this case a modified Fourier transform which reduces systematical error by using a fit function.

To our best knowledge the current state-of-the-art is an array of MRRs that can be measured one-by-one using grating couplers [4]. This system can only measured every sensor once every few seconds and requires an advanced setup to allow for automatic coupling light in and out of the grating couplers. The work in this thesis describes a system that is truly multiplexing, making it possible to measured every sensor at the same time without having to

INTRODUCTION

realign between every measurement. The focus of this thesis is on determining if the concept of multiplexing works with refractive index sensors.

1.2 OUTLINE

This thesis is structured as follows. Chapter 2 discusses the fundamental theory required to explain the basic concept of integrated refractive index sensors. Chapter 3 discusses the signal processing that retrieves the change in refractive index from the measured signal. Chapter 4 continues on the topic of Chapter 2 and discusses a measurement to support the theory. Chapter 5 discusses the multipath interferometer refractive index sensor. Chapter 6 discusses an advanced property of the MRR.

THEORY OF INTEGRATED PHOTONIC REFRACTIVE INDEX SENSORS

This chapter describes the theory of refractive index (RI) sensors and in particular for the sensors based upon an integrated Mach-Zehnder interferometer (MZI) or a microring resonator (MRR). The responsivity for both types of sensor is derived and the influence of temperature change on sensor performance is analysed.

2.1 REFRACTIVE INDEX SENSOR

The refractive index is a material property describing the linear response of a medium to an applied EM field (typically an optical wave) and equals to the ratio of the phase velocity of light in vacuum to that in the medium. The refractive index of a medium is dependent on the materials, temperature, pressure and stress. This allows translating a change in refractive index into one of these other properties. Therefore, by measuring the change in refractive index, a change in one of these properties can be measured as long as the remaining properties are kept constant. A device that measures the refractive index is called a RI sensor.

This work focuses on integrated optics and in particular on microring resonator and Mach-Zehnder interferometer based RI sensors. Inside the MZI the light is divided over two different arms, the sensing and reference arm, as seen in figure 1. Light propagating along the sensing arm interacts with the medium of interest and the light propagating along the reference arm is confined within the cladding and does not interact with the medium of interest. As part of the optical field of the propagating mode through the sensing arm experiences the refractive index of the material of interest, the effective refractive index of the mode changes and so does its propagation phase. When this light interferes with the light propagated along the reference arm at the output waveguide, a power modulation as function of the phase difference results.

Various processes are responsible for changing the RI of the material above the sensing window. Examples are a varying alcohol content in water or a specific type of molecule that binds to a biochemical layer on top of the waveguide in the sensing window.

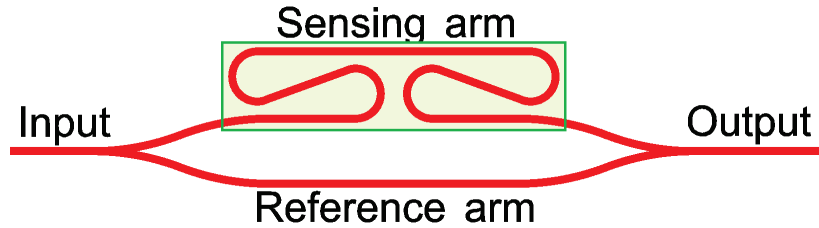


Figure 1: A schematic representation of a Mach-Zehnder Interferometer (MZI) with a sensing window. The position of the sensing window is given by the rectangle. Light from the input is divided over the reference arm and sensing arm. The light in each arm has a different phase shift depending on the optical path-length, combining these two light fields in the output waveguide results in interference. The intensity of this interference signal varies with the refractive index and the wavelength of the light. A change in refractive index in the sensing window results in a measurable intensity change at a fixed wavelength.

The Mach-Zehnder interferometer (MZI) is a two-path interferometer. A typical implementation as integrated photonic sensor is shown in figure 1. In interferometers the output is determined by the superposition of the light fields that have taken, in this case, two different paths and are combined into the output waveguide. When describing the MZI both the terms arm and path are used. Path refers mainly to the optical path, including the effective refractive index that is affecting the light propagating through this path., while arm refers mainly to the physical waveguide. The intensity obtained as result of this superposition is related to the phase difference $\Delta\phi$ of the light waves traveling through the two arms of the MZI. If $\Delta\phi$ is equal to zero or modulo 2π , then constructive interference occurs, resulting in a maximum in intensity at the output [5]. If $\Delta\phi$ is equal to modulo π , then destructive interference occurs, resulting in a minimum in the intensity at the output. So when the phase difference $\Delta\phi$ changes the intensity in the output waveguide will cycle through a minimum and maximum power. Because of this, the phase difference $\Delta\phi$ can only be uniquely determined within an interval of π . At a fixed wavelength it is only possible to change the phase difference $\Delta\phi$ between these light waves by changing the effective RI experienced by the light propagating along these paths, so a structure like this can be used to determine the RI.

The phase difference $\Delta\phi$ can be determined by measuring the intensity in the output for a certain $\Delta\phi$. The maximum intensity for $\Delta\phi$ equals to modulo $s\pi$ and the minimum intensity when $\Delta\phi$ equals to modulo π . However it is easier to make the MZI's output wavelength dependent and have multiple maximum and minimum intensities in the measured wavelength range. In order to make the MZI's output wavelength dependent over a small wavelength range, the path-length difference between the two paths should be larger than the wavelength. An representation of a resulting wavelength spectrum is shown in figure 2. In this figure the vertical axis is the power resulting from interference the interference signal measured by a photo detector. The horizontal axis is the wavelength difference $\Delta\lambda_m$ around a center wavelength λ , with $\lambda \gg \Delta\lambda$. This condition is required, because the wavelength spectrum of the MZI is only periodic as function of light frequency. But for a small wavelength range it is also assumed to be periodic. This figure shows two wavelength spectra, representing the wavelength spectrum before and after a refractive index change.

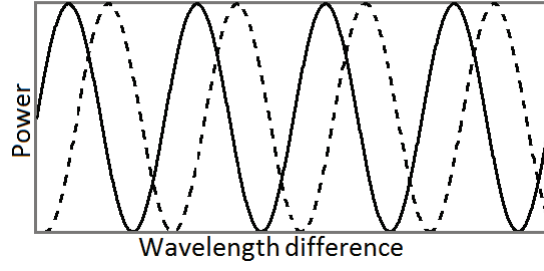


Figure 2: Schematic view of wavelength spectra of a Mach-Zehnder interferometer with a path-length difference between both arm that is a lot larger than the center wavelength. In this figure the power on the y-axis is a result of the interference of the light waves from these two arms as measured by an optical power detector. The wavelength difference on the x-axis is describing a small wavelength range $\Delta\lambda$ around a center wavelength λ , with $\lambda \gg \Delta\lambda$. The solid and dashed lines correspond to two different values for the effective refractive index of the sensing arm, by determining the phase or wavelength shift between these lines the change in effective refractive index can be determined.

2.3 THEORY OF THE MACH-ZEHNDER INTERFEROMETER

The performance of a refractive index sensor is characterized by its sensitivity. The sensitivity is defined as the minimum detectable change in refractive index. This is determined by the measurement error divided by the responsivity of the sensor. This measurement error consist of both noise and time dependent errors, this is discussed in more detail in chapter 4. The responsivity is the amount of output signal per unit of input signal. For the MZI responsivity is either the amount of wavelength spectrum shift $\partial\lambda_m$ or phase change $\partial\theta$ per unit of refractive index. This is done by first understanding the phases involved in this interference and then by finding the relation between the phase difference and the refractive index change. For the MZI, interference is caused by the difference in phase that the two light waves have acquired when propagation through two two arms of the MZI. The light propagation through the reference arm acquired a phase shift ϕ_r given by the physical length L_3 of the waveguide multiplied with the effective refractive index n_r ,

$$\phi_r = kn_r L_3. \quad (1)$$

Here k is the wavenumber $\frac{2\pi}{\lambda}$ and λ is the vacuum wavelength of the light. The light propagating through the sensing arm goes through a waveguide that passes through the sensing window and this light also goes through a waveguide outside of the sensing window. Therefore, the phase ϕ_s of the light going through the sensing arm at a fixed wavelength is given by the physical length L_1 of the waveguide outside the sensing window multiplied with the corresponding effective refractive index n_r , plus the physical length L_2 of the waveguide passing through the sensing window multiplied with the corresponding effective refractive index n_s ,

$$\phi_s = kn_r L_1 + kn_s L_2. \quad (2)$$

The phase difference $\Delta\phi$ can now be expressed as the difference between these two phases,

$$\Delta\phi \equiv kn_r(L_1 - L_3) + kn_s L_2. \quad (3)$$

The amount of change in the phase difference $\Delta\phi$ between light from the two arms when the effective refractive index n_s changes is given by the derivative,

$$\frac{\partial\Delta\phi}{\partial n_s} = kL_2. \quad (4)$$

With the data processing described in chapter 3, $\partial\Delta\phi$ follows directly from the MZI's output signal. However, the common notation is to have the responsivity in wavelength spectrum shift rather than a phase shift. When the measured wavelength spectrum has a phase shift $\partial\Delta\phi$ of 2π , then the measured wavelength spectrum has a wavelength shift equal to the distance between two successive maximums, this distance is called the free spectral range FSR . The phases for two successive maximums are,

$$\Delta\phi = \frac{2\pi}{\lambda}(n_r(L_1 - L_3) + n_s L_2) \quad (5)$$

and

$$\Delta\phi + 2\pi = \frac{2\pi}{\lambda - FSR}(n_r(L_1 - L_3) + n_s L_2). \quad (6)$$

Inserting equation 5 into equation 6 gives,

$$FSR = \frac{\lambda^2}{\lambda + (n_r(L_1 - L_3) + n_s L_2)}. \quad (7)$$

Now we apply the condition $|\frac{(n_r(L_1 - L_3) + n_s L_2)}{\lambda}| \gg 1$. The reason for this condition is that we need the measured wavelength spectrum of our MZI to have at least one minimum and maximum in intensity. With other words, the measured wavelength spectrum should contain at least half a FSR . The drawback for this condition is that one arm has to be longer than the other arm, resulting in the first condition for a minimum arm length difference. For this case, the FSR becomes,

$$FSR = \frac{\lambda^2}{(n_r(L_1 - L_3) + n_s L_2)}. \quad (8)$$

In order to determine the shift in wavelength of the modulated output power, we define λ_m as the wavelength corresponding to a maximum in intensity in the MZI's output. Using equation 3, the responsivity can now be written as,

$$\frac{\partial\lambda_m}{\partial n_s} = \frac{\partial\lambda_m}{\partial\Delta\phi} \frac{\partial\Delta\phi}{\partial n_s} = \frac{FSR}{2\pi} \frac{2\pi L_2}{\lambda_m} = \frac{L_2 \lambda_m}{n_r(L_1 - L_3) + n_s L_2}. \quad (9)$$

This result shows that the responsivity in wavelength shift is dependent on the path-length difference and the responsivity can be increased by reducing this path-length difference. A typical value for the responsivity for optical chips used in this work is 110 nm per RI unit when $L_1 - L_3$ equals to zero. However the responsivity in phase shift is only dependent on the length L_2 . So far it is not possible to determine if a larger responsivity has any effect on the sensitivity, because the measurement error might also scale with responsivity.

2.4 MZI THEORETICAL PERFORMANCE

In section 2.1 it was mentioned that the RI depends on multiple physical parameters, two of these are the material concentrations and temperature. For instance the MZI can be used as RI sensor when a solution of varying content of alcohol in water is placed in the sensing window. But the RI sensor also measures a response when the temperature changes. This makes it possible to use the MZI for multiple purposes, but in most cases it is undesired to measure the RI change of the liquid in the sensing window and the temperature at the same time. This section discusses the three MZI designs in their performance to measure only one RI contribution and not the other contributions. The first design is a MZI without a sensing window. This MZI design is shown in figure 3 and is called a blind MZI. The sensor's temperature is assumed to be homogeneous. If this assumption holds in practice is determined in chapter 4.

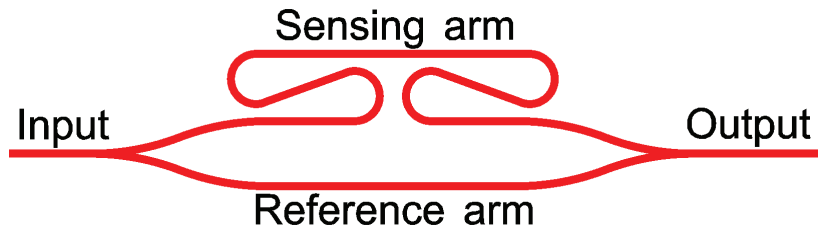


Figure 3: Schematic representation of a MZI without a sensing window. A global homogeneous temperature change causes a global refractive index change on the MZI.

When working with a homogeneous temperature change it is not possible to isolate the reference arm from the sensing arm, this means that the RI of both arms changes with temperature. But different materials are affected differently by temperature. The blind MZI uses the same materials everywhere, which means that the effective refractive index is the same everywhere,

$$n_r = n_s. \quad (10)$$

Because both arms have the same refractive index, equation 3 simplifies,

$$\Delta\phi = kn_r\Delta L \quad (11)$$

Where ΔL is the arm length difference. Just as in the previous section this can be rewritten into a shift in MZI's wavelength spectrum $\partial\lambda_m$. But in this case the effective refractive index change is caused by temperature T , so the temperature response is given by,

$$\frac{\partial\lambda_m}{\partial T} = \frac{\lambda_m}{n_r} \frac{\partial n_r}{\partial T} \quad (12)$$

In the derivative of equation 12, the thermal expansion has been ignored, because this will only work on the path-length difference, effectively multiplying $\partial\lambda_m/\partial T$ with a certain factor. Equation 12 shows that the blind MZI response to temperature is independent of path-length difference, unlike equation 9, where the responsivity could be increased by decreasing the path-length difference. So far no measurement errors have been discussed, only temperature and a change in the sensing window's effective refractive index n_s , this makes it not possible to give a performance of this design. The only thing that can be said is that the blind MZI has no sensing window, so this design is ideal for measuring only temperature.

The second design is represented in figure 1. This is the design that was used in section 2.2 has a sensing window unlike the blind MZI. This also means that the sensor has a different temperature dependence in the sensing arm compared to the reference arm. The responsivity caused by a change in n_s is shown equation 9. For the temperature responsivity we start from equation 3.,

$$\frac{\partial \lambda_m}{\partial T} = \frac{\partial \lambda_m}{\partial \Delta \phi} \left(\frac{\partial n_s}{\partial T} \frac{\partial \Delta \phi}{\partial n_s} + \frac{\partial n_r}{\partial T} \frac{\partial \Delta \phi}{\partial n_r} \right) = \frac{(L_2 \frac{\partial n_s}{\partial T} + (L_1 - L_3) \frac{\partial n_r}{\partial T}) \lambda_m}{n_r(L_1 - L_3) + n_s L_2}. \quad (13)$$

Typically, the two responsivities $\frac{\partial n_s}{\partial T}$ and $\frac{\partial n_r}{\partial T}$ will have a different temperature dependence. This causes the temperature responsivity of this sensor to be dependent on the total arm lengths. So both equation 13 and equation 9 are dependent of the lengths of the MZI's arms. This means that any design choice to increase responsivity for ∂n_s will increase the responsivity to temperature ∂T as well, which is not ideal as sensor.

The third design from figure 4 has both the reference and sensing arm passing through the sensing window for the same length. While the additional path-length required to obtain the *FSR* requirement is outside of the sensing window. This means that this structure does not react to a effective refractive index change ∂n_s , but the inner rectangle in this figure represents an biochemical layer placed on top of waveguide that allows for specific molecules to bind to it.

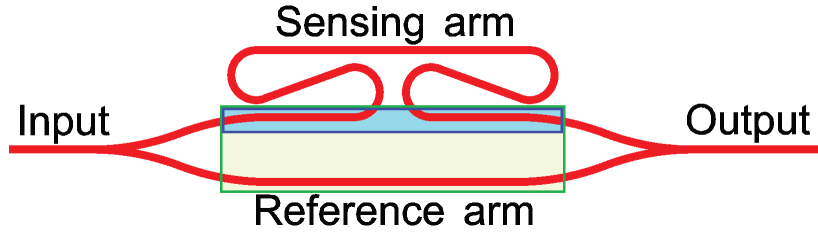


Figure 4: Schematic representation of a MZI with a large sensing window covering both arms of the MZI. A global homogeneous temperature change causes the same refractive index change on both arms. The green outer rectangle illustrates the sensing window. The blue inner rectangle illustrates the biochemical layer for molecule binding. This layer itself and the molecules binding onto it cause a small effective refractive index change, it is assumed that this small change does not drastically affect the response to temperature of the whole cross section.

The response to an effective RI change caused by molecule binding can be derived similar how equation 9 was derived, while the responsivity to temperature is the same as equation 12, assuming that the small change in RI due to molecule binding does not drastically affect the response to temperature of the whole cross section. This means that the temperature responsivity is independent on the path-length, while the responsivity to an effective refractive index change caused by molecule binding can be increased with path-length passing through sensing window that has this biochemical layer.

So in conclusion the blind MZI can only measure temperature since the optical fields propagating through the waveguides in this sensor are completely isolated from external refractive

index changes. The third design is the ideal sensor to measure a the concentration of a specific molecule. However, only the second design can be used to measure an effective refractive index change in the sensing window when molecule binding is not possible.

2.5 INTRODUCTION TO MICRORING RESONATOR



Figure 5: Schematic representation of a microring resonator (MRR). Light from the input is coupled in and out of the MRR with a directional coupler.

The microring resonator (MRR) is a resonator created by having a waveguide coupled onto itself. Light can be coupled in and out of the MRR with a directional coupler. In figure 5 light from the input is for a part coupled to the MRR, the other part goes to the through port. This also means that light inside the MRR is partly coupled out and partly going for another round. The amount of light being coupled depends on the interference between the light from the input and the light inside the MRR. When the MRR is in resonance, then the intensity inside the MRR is maximal and propagation losses causes the intensity in the through port to be minimal. This resonance condition occurs when the wavelength of the guided light fits an integer number of times in the vacuum length of the MRR. The MRR can be used as refractive index sensor just as the MZI. When the effective refractive index of the MRR changes, then the resonances shift in wavelength. In the following section the responsivity of the MRR is determined.

2.6 THEORY OF THE MICRORING RESONATOR

For the MZI the phase difference was caused by the optical path-length difference between the two arms. In case of the MRR, light inside the MRR can propagate through the MRR for multiple round trips. This causes for a large amount of interferences between the multiple round trips of the light from the MRR and light from the input. These interferences are only affected by the roundtrip phase and amplitudes. The exact response from the MRR is given in the book of Okamoto [5] and a schematic view of the response is shown in figure 6. The roundtrip phase is defined as,

$$\Delta\phi = knL_{ring}. \quad (14)$$

Here k is defined as the wavenumber $\frac{2\pi}{\lambda}$, where λ is the vacuum wavelength. L_{ring} is the physical length of the MRR. We are interested in the change in phase difference $\partial\Delta\phi$ when the effective refractive index n of the MRR changes. This is obtained by taking the derivative of equation 14 to n ,

$$\frac{\partial\Delta\phi}{\partial n} = kL_{ring} \quad (15)$$

Just as for the MZI this can also be translated to the wavelength shift by using the FSR (distance between neighboring maximums) from equation 8 with L_1 and L_3 both zero. In this

equation λ_m refers to a wavelength for which a maximum in intensity is obtained. This results in a wavelength responsivity defined as,

$$\frac{\partial \lambda_m}{\partial n} = \frac{\partial \lambda_m}{\partial \Delta \phi} \frac{\partial \Delta \phi}{\partial n} = \frac{FSR}{2\pi} \frac{2\pi L_{ring}}{\lambda_m} = \frac{\lambda_m^2}{n L_{ring}} \frac{L_{ring}}{\lambda_m} = \frac{\lambda_m}{n}. \quad (16)$$

Equation 16 shows that the wavelength shift per effective refractive index change is constant for any practical effective refractive index change and for a small wavelength range around a center vacuum wavelength, where the wavelength range is a lot smaller than this vacuum wavelength. A typical value for the responsivity for the optical sensors used in this work is 110 nm per RI unit. This means that the responsivity of any MRR is the same for every geometric length, however the FSR is dependent on the round trip length of the MRR. This responsivity will be discussed in the last paragraph of this section. We first have to take into account that the interference consists of light coming from many different optical path-lengths. In figure 6 it can be seen that the full width at half maximum (FWHM) of the spectrum relative to its FSR is smaller than that of the MZI. A MRR with low total loss will give a spectrum with very narrow dips. For a flank detection algorithm it might be enough to measure over a wavelength range of about twice the FWHM, allowing to make MRRs smaller than the minimum size of MZIs. But in practice it is quite challenging to use such small MRRs, because the measured wavelength range has to shift in wavelength to keep track of the resonance condition, resulting in an additional source of error. If more than a single FSR is measured, then a the another resonance condition will enter the wavelength range when one shifts out. And if the input light is varied in wavelength, rather than a spectrometer at the output, than the light source can be used for multiple sensor, as long as at least one FSR is measured. For this work there is no need for such small MRRs and we want to measure multiple MRRs with the same light source. So the boundary condition for the smallest MRR is set to be the length required to obtain one FSR or more, this length can be obtained from equation 8.

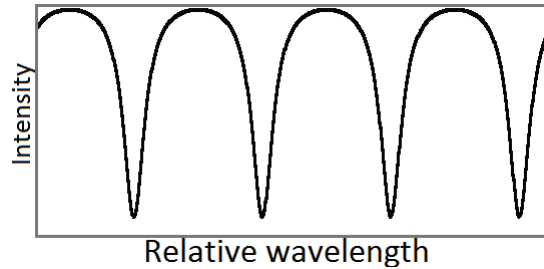


Figure 6: Schematic view of the wavelength spectrum of a microring resonator (MRR). The intensity on the vertical axis is the resulting intensity in the output coming from the interferences. The wavelength on the horizontal axis is describing a small wavelength range $\Delta \lambda$ around a center wavelength λ_m , with $\lambda_m \gg \Delta \lambda$.

The response of the MRR to temperature compared to an effective refractive index change caused by varying material concentrations is similar to that of the second MZI example, where only one arm had a sensing window and with a zero-length reference arm. For the MRR it is not possible to have any modification to increased responsivities to either one of the effective refractive index changes. But just as the MZI the responsivity of the phase shift $\partial \Delta \phi$ does increase with the length of the MRR, the advantage of this is explained in chapter 3. So far it is not yet determined if an increase in responsivity also means an increase in sensitivity, so

the measurement errors have to be known first before being able to compare sensors, this is discussed in chapter 4.

 SIGNAL PROCESSING

Refractive index (RI) sensors are used to measure how a RI of interest changes with time. The measurement gives a measured wavelength spectrum that shift in time. However, the desired parameter of interest is the phase ϕ of this spectrum. In this chapter the data processing algorithm is analyzed.

As shown in equation 4 and equation 15 a change in refractive index ∂n causes for a shift in phase difference $\partial\Delta\phi$ between light waves. A good method of determining a phase of a periodic signal is by using an algorithm based on the Fourier transform. This algorithm has as input or measured power as function of wavelength and as output the phase shift $\partial\Delta\phi$ relative to a reference measurement.

This chapter begins with the Fourier transform (FT) which for instance can decomposes a function of time into the frequencies that make it up, with corresponding phases. The FT can also link other domains, for example normal space and reciprocal space. As the most common application of the FT is to transform between the time and frequency domains, some of the properties of the FT will be discuss using these domains. The FT is a simple technique that works best if all the frequency functions in the input function are orthogonal, as will be explained in the next section. The second algorithm is the Least Squares Error (LSE) fit. This is an algorithm that is similar to the FT for periodic signals, but it takes in account that the input function consist of non-orthogonal frequency functions. The third section consist of the error analyses.

3.1 FOURIER TRANSFORM

In 1822 Joseph Fourier introduced the Fourier transform for the first time [1]. This is a technique that shows that any real function can be written as an infinite sum of sines and cosines. The transform in one direction for one element of this infinite sum is given by,

$$Y(f) = \int_{-\infty}^{+\infty} (y(t)isin(2\pi ft) + y(t)cos(2\pi ft))dt. \quad (17)$$

In this case $Y(f)$ is the Fourier transform of $y(t)$. Where t is the time and f is the frequency.

In the case of RI sensors, the signal is measured as function of inverse-wavelength differences X , where X is defined as $0 \dots X_{max}$, X_{max} is $\frac{1}{\lambda_{min}} - \frac{1}{\lambda_{max}}$, λ_{max} is the maximum wavelength of the wavelength range and λ_{min} is the minimum wavelength of the wavelength range. From here on it is important to use inverse-wavelength, because over a large wavelength range the FSR is not constant, as described in chapter 2. For a small wavelength range it might be considered constant, but even in that case it does not require much effort to use inverse-wavelength instead of wavelength. The only effort required is that the array X should be uniformly sam-

pled. We want the output of the Fourier transformed power FT_P to be a function of optical path-length difference ΔL_{opt} , as the inverse of inverse-wavelength has the unit for length.

The FT multiplies the input function by a sine and cosine function. In the time-to-frequency transform the sine function is $\sin(2\pi ft)$. In this case we substituted and normalized the time t for $\frac{X}{X_{max}}$. The frequency f is substituted for $\frac{\Delta\lambda_m}{FSR}$,

$$\sin(2\pi \frac{X}{X_{max}} \frac{\Delta\lambda_m}{FSR}). \quad (18)$$

The FT's input function $P(X)$ is a periodic signal measured from λ_{min} till λ_{max} and could for example be the output signal of the MZI or MRR. The intensity P is measured over an inverse-wavelength range at discrete value, this makes it possible to write the infinite integral as a finite sum. The Fourier transform for this case is given by,

$$FT_P(\frac{\Delta\lambda_m}{FSR}) = \sum_{X=0}^{X=1} (P(X) \sin(2\pi \frac{X}{X_{max}} \frac{\Delta\lambda_m}{FSR}) + P(X) \cos(2\pi \frac{X}{X_{max}} \frac{\Delta\lambda_m}{FSR})). \quad (19)$$

In equation 19 the "time" is normalized between 0 and 1 and dimensionless, because of this the "frequency" will give the number of periods in the input, or more precise, the number of times the FSR fits in the wavelength range $\Delta\lambda_m$. Instead we want to multiply this value $\frac{\Delta\lambda_m}{FSR}$ by a conversion factor C that converts it to optical path length difference. Assume C would equal to 1, then $\frac{\Delta\lambda_m}{FSR}$ will give the number of periods that the envelope of the intensity P has. Instead we want to give C a value such that $\frac{\Delta\lambda_m}{FSR} C$ will give the optical path-length difference ΔL_{opt} , using equation 8. If $\frac{\Delta\lambda_m}{FSR}$ is 1, then $\Delta\lambda_m = FSR$. This can be rewritten to $\Delta\lambda_m = \frac{\lambda_m^2}{\Delta L_{opt}}$. If $\frac{\Delta\lambda_m}{FSR}$ equals to a real number N , then $\Delta\lambda_m = N FSR$. This can be rewritten to $\Delta\lambda_m = N \frac{\lambda_m^2}{\Delta L_{opt}}$. In this case ΔL_{opt} is N times larger, then the ΔL_{opt} required for $\Delta\lambda_m = FSR$. This means that the conversion factor C equals to the ΔL_{opt} required to obtain $\Delta\lambda_m = FSR$, so C is given by,

$$C = \frac{\lambda_m^2}{\Delta\lambda_m}. \quad (20)$$

So that the result becomes,

$$FT_P(\Delta L_{opt}) = FT_P(\frac{\Delta\lambda_m}{FSR} C). \quad (21)$$

In general the Fourier transform is used to obtain a frequency spectrum. This can be done by repeating the transformation from equation 17 or 19 for all frequencies or path lengths. In the case of a refractive index sensor ΔL_{opt} are known as long as the refractive index changes remain small, or $\frac{\Delta\lambda_m}{FSR}$ can easily be obtained from the signal. So the Fourier transform only has to be calculated for a the number path length difference in the sensor or till the amplitude of that interference is neglectable. This makes the Fourier transform requires little computational power.

The last step is to determine the phase change $\partial\Delta\phi$ of the FT's input function. For this

we measure the power as function of wavelength and determine the phase θ . Then we do a second measurement some time later and take the FT of that measurement. From this we retrieve a second phase. The difference between these phases reflect the change in effect refractive index in the sensing arm. The equation used to obtain the phase is given by [3],

$$\theta = \tan^{-1}\left(\frac{-\text{imag}(FT_I)}{\text{real}(FT_I)}\right). \quad (22)$$

For this application the FT is not ideal, because non-orthogonal frequency functions from the FT's input function affect each other's amplitude after the FT. Frequency functions are orthogonal when the dot product is zero. For example, take equation 17, with $y(x)$ a function of x that contains an integer number of periods of a sine wave and has an offset. x is finite and goes from 0 to 1. In this case the frequency of interest f is an integer, so the dot products of $\sin(2\pi fx)$ and $\cos(2\pi fx)$ with the offset gives zero. In this case the frequency component of interest in the function is orthogonal with the other frequency component in the function, namely the offset. Because they are orthogonal they can not affect each other.

For another example take equation 17, with $y(x)$ a function that contain an non-integer number of periods of a sine wave and has an offset. x is finite and goes from 0 to 1. In this case the frequency of interest f is not an integer, so the dot products of $\sin(2\pi fx)$ and $\cos(2\pi fx)$ with the offset will not give zero. The frequency component of interest in the function is not orthogonal with the other frequency component in the function, so the offset will affect the frequency component of interest in the Fourier transformed function. This interacting is an unwanted error and this error can be determined by the Fourier transform in order to correct for it. This correction does require prior knowledge of all frequency components in the function, turning the algorithm into a fitting algorithm as shown in the next section.

3.2 LEAST SQUARED ERROR FIT

The least square estimation (LSE) fit [3] is an algorithm that can fit linear function in a single iteration. Non-linear functions are also possible, but require multiple iterations. In the work the fit function is a sinusoidal functions, because the measured response function of the RI sensor is periodic. This means that this algorithm has to fit a linear sin and cosine function for every path-length difference, just as the FT did. The alternative would be to fit a single sine function with a phase, but that is a non-linear function, greatly increasing the processing time.

Going back to the example in the previous section, the input function $y(x)$ consists of a known frequency f with an unknown amplitude, phase and an offset with unknown amplitude. As said in previous paragraph it is not possible to have the phase as fit parameter directly, so the trick from equation 22 has to be used, where a sine and cosine function can be used to obtain a phase of a given frequency. This gives a fit function $y_{fit}(x)$ with 3 fit parameters A , B and C ,

$$y_{fit}(x) = A \sin(2\pi fx) + B \cos(2\pi fx) + C. \quad (23)$$

The way this algorithm works is by determining the fit variables so that the difference between the input function and the fit function is zero. So the LSE fit is defined as,

$$\sum_{x_{min}}^{x_{max}} [y(x) - y_{fit}(x)]^2 = 0. \quad (24)$$

This can be solved using matrices. We define the matrix D as the arrays of $\sin(2\pi fx)$, $\cos(2\pi fx)$ and 1. The array F consisting of the fit variables.

$$D = \begin{pmatrix} \sin(2\pi fx_{min}) & \cos(2\pi fx_{min}) & 1 \\ \vdots & \vdots & \vdots \\ \sin(2\pi fx_{max}) & \cos(2\pi fx_{max}) & 1 \end{pmatrix}, F = \begin{pmatrix} A \\ B \\ C \end{pmatrix}, y = \begin{pmatrix} y(x_{min}) \\ \vdots \\ y(x_{max}) \end{pmatrix} \quad (25)$$

Inserting the definitions from equation 25 into equation 24 results in,

$$(y - DF)^T(y - DF) = 0 \quad (26)$$

This can be rewritten into,

$$F = (D^T D)^{-1}(D^T y) \quad (27)$$

Where $(D^T y)$ may be recognized as the Fourier transform as given in equation 19. And $(D^T D)^{-1}$ acts as a correction matrix. The phase $\partial\Delta\phi$ can now be determined by using the fit variables A and B from F into equation 22.

3.3 ERROR ANALYSES FOR NOISE

When determining the phase shift θ there are many sources of error. The two categories of errors are random and systematic errors. In this work we define random errors as unpredictable in nature and have the property that they are zero when averaged. All unpredictable errors in this work are also statistical in nature, but all statistical errors are not unpredictable. A predictable error is one of the systematic error and can be compensated for. A common random errors are intensity and wavelength noise, this is an error for which is amount of error can be determined, but it cannot be removed. An example of a systematic error would be a fluctuating chip temperature, because this error can be measured with a second sensor and compensated for. Therefore, the accuracy of the measurement is ultimately determined by the errors that can not be compensated for. A property from intensity and wavelength noise is that it gives a phase error, this means that this error is not depending on the FSR . While an error such as chip temperature is for a blind sensor is the same for every sensor in wavelength noise.

The following algorithm is used to quantify the amount of phase θ error caused by intensity and wavelength noise. As explained, the random errors ultimately determine the measurement accuracy, but when the total error is larger than the error caused by random errors, then the systematic errors have not been fully compensated for.

The standard deviation of the phase θ over a time interval is defined as,

$$\sigma_\theta \equiv \sqrt{\frac{(\theta(t) - \theta_{mean})^2}{M - 1}} \quad (28)$$

Where M is the number of data points in $\theta(t)$.

For determining the expected error caused by random errors the first task is to obtain the standard deviation of the noise. This is obtained by removing all non-random signal from the measured signal. So to obtain the noise, the fitted function $P_{fit}(\lambda)$ is subtracted from the measured signal $P(\lambda)$. In practice this will not have removed all non-periodic signal, because of

remaining systematical error or because the fit function is not describing the measured signal perfectly. To remove the rest of the non-periodic signal the residue $r(\lambda)_m = P_m(\lambda) - P_{fit,m}(\lambda)$ is subtracted by the residue $r(\lambda)_{m-1} = P_{m-1}(\lambda) - P_{fit,m-1}(\lambda)$, where m refers to measurement m , $m - 1$ refers to the measurement prior to measurement m . The remaining residue is the sum of two noise signal, resulting in a standard deviation that is a factor $\sqrt{2}$ larger than that of a single signal, so the remaining residue is divided by this factor. The final residue $R(\lambda)$ is given by,

$$R(\lambda) = \frac{1}{\sqrt{2}}(r(\lambda)_m - r(\lambda)_{m-1}) \quad (29)$$

This equation is demonstrated in the simulation in figure 7. In this figure $P_m(\lambda)$ is simulated as a function that is not perfectly periodic or normalized. Figure 7B shows $P_{m,fit}(\lambda)$ using the same fit function as given by equation 25. Figure 7D shows the residue $r_m(\lambda)$ that is obtained after subtracting the raw signal with its fit. The same has been done for a second input $P_{m-1}(\lambda)$ as shown in figure 7C and 7E. The final residue $R(\lambda)$ is shown in figure 7F. The figure also shows that the standard deviation obtain from $R(\lambda)$ is very close to the standard deviation of the input noise.

With this obtained residue, the standard deviation is calculated using the variance in multiple linear regression technique.

$$\sigma_{F,j} = \sigma_R \sqrt{([D^T D]^{-1})_{jj}} \quad (30)$$

In this equation j stands for the array index, jj for the matrix diagonal and σ_F stands for the final standard deviation. The outcome of this equation are the standard deviations of the fit variables. These are used to calculate the standard deviations in the phase θ ,

$$\sigma_\theta^2 = \left(\frac{\partial\theta}{\partial A}\right)^2 \sigma_A^2 + \left(\frac{\partial\theta}{\partial B}\right)^2 \sigma_B^2 \quad (31)$$

The definition for $\partial\Delta\phi$ is in equation 22. Evaluating the partial derivatives and inserting those in equation 31 gives,

$$\sigma_{\partial\Delta\phi} = \frac{1}{1 + \left(\frac{B}{A}\right)^2} \sqrt{\left(\frac{B}{A^2}\right)^2 \sigma_A^2 + \left(\frac{1}{A}\right)^2 \sigma_B^2} \quad (32)$$

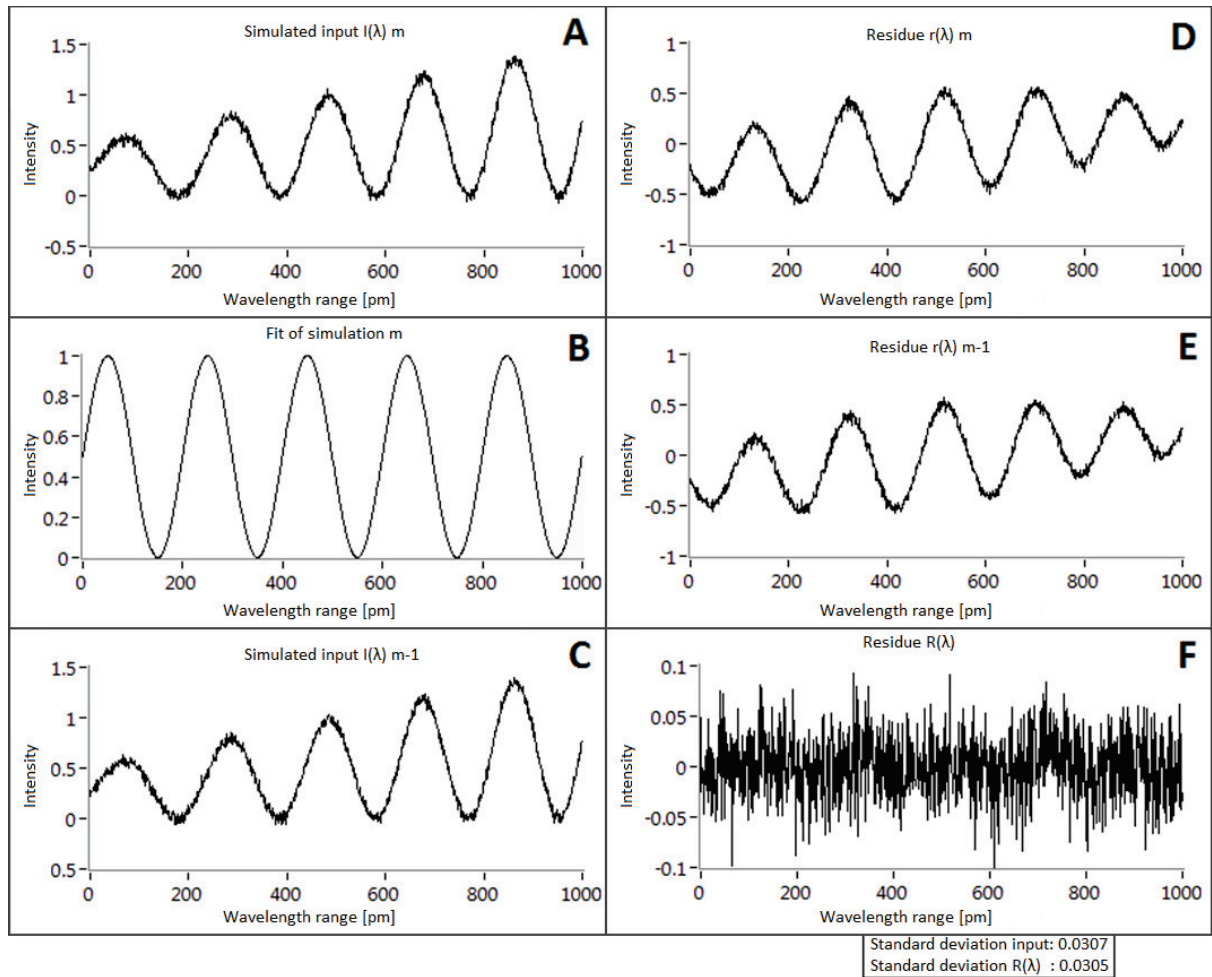


Figure 7: This figure illustrates how the algorithm extracts the random noise out of a measured signal. (A) is a simulated input which is not normalized and not perfectly periodic, representing a real measurement. (B) this is the fitted function from (A) using the fit variables as given in equation 25. In (D) the residue from subtracting (B) from (A) is shown. (C) this shows a second simulated input signal and (D) shows the corresponding residue. In (F) the final residue is shown obtained by subtracting (E) from (D). It can also be seen that the standard deviation in (F) is nearly the same as the standard deviation of the simulated input noise.

 USABILITY OF MZI AND MRR

4.1 MZI COMPARISON BASED ON THEORY

In chapter 2 the theory of the MZI was discussed, but it did not give any conclusion to which parameter affects the sensor positively. However that chapter did say that temperature could have less effect on the MZI when $L_3 - L_1$ is increased. To get a better feeling for this statement, three MZI structures are compared in theory, all with the configuration as shows in figure 4. The first MZI with a small FSR, $L_3 - L_1 = 0$. The second MZI has a large free spectral range (FSR) with $0 < L_3 - L_1 < L_2$, this increasing both the size of as sensor as well as the wavelength responsivity $\frac{\partial \lambda_m}{\partial n_s}$. The third MZI has a longer interaction length L_2 , causing the phase responsivity $\frac{\partial \Delta \phi}{\partial n_s}$ to increase as well as the sensor size.

In the following equations, σ refers to the standard deviation of a certain error. So σ_{noise} refers to the amount the wavelength spectrum shift $\partial \lambda_m$ shifts around its mean value of $\partial \lambda_m$ in a stable situation. Where a stable situation refers to a situation where time averages of the refractive index, temperature and sensing window refractive index remain constant.

The light being send through these sensors is coming from a light source which sweeps its wavelength in time. This means that it has a center wavelength and a wavelength scan range. The light coming out of the chip is measured by a photo detector in time. These components are triggered at a different times, because the light source requires a short start up time. The errors that can occur in this system is that the trigger timing can fluctuate, causing the measured center wavelength to shift. The VCSEL temperature could fluctuate, which we assume to be a slow fluctuations that mainly causes the center wavelength to shift. For simplicity we assume the wavelength sweep to have a constant wavelength scan range, but a the center wavelength that can fluctuate in time around the mean center wavelength. The standard deviation of this fluctuation is σ_{scan} . This error is completely independent on the chip, which has as advantage than when measuring a second sensor in parallel with the same light source, that both sensor obtain the same wavelength shift. So a second sensor measured parallel can be used

The third type of error considered here is the global temperature fluctuation σ_T of the chip. We still assume the temperature to be homogeneous and to only affect the path-length difference. In the next section we determine if this assumption is correct.

In this theoretical experiment the sensitivity S of the sensors is determined by dividing the total error by the responsivity $\frac{\partial \lambda_m}{\partial n_s}$. The time scale of the errors contributing to the total error are all different, therefore we define the total error as the sum of all contributing error.

First the MZI-with-small-FSR, which resulting sensitivity is the reference to which we compare the other sensors.

$$S_1 = (\sigma_{noise} + \sigma_{VCSEL} + \sigma_T) \frac{1}{\frac{\partial \lambda_m}{\partial n_s}}. \quad (33)$$

For the MZI-with-large-FSR we take that the FSR is reduced by a factor of 10. This causes the responsivity $\frac{\partial \lambda_m}{\partial n_s}$ to be 10 times large. The MZI's modulation frequency as function of wavelength becomes 10 times small, which increase the wavelength noise by a factor of 10. The sensor does not affect the other components in the systems, so σ_{scan} is unaffected. σ_T is reduced by a factor of 10, because the path-length difference is reduced by this factor.

$$S_2 = (10\sigma_{noise} + \sigma_{scan} + \frac{\sigma_T}{10}) \frac{1}{10 \frac{\partial \lambda_m}{\partial n_s}} = (\sigma_{noise} + \frac{\sigma_{scan}}{10} + \frac{\sigma_T}{100}) \frac{1}{\frac{\partial \lambda_m}{\partial n_s}} \quad (34)$$

From the result of equation 34 compared to equation 33 it can be seen that in this situation the error σ_{noise} cause by noise is unaffected. This means that reducing the *FSR* is only useful when the error by noise is not dominant over the other errors. σ_{scan} is reduced by a factor of 10, which comes without any direct downside. In this result σ_T did decrease by a factor of 100, but the assumption of a homogeneous temperature becomes questionable when making the sensor larger.

For third MZI we double the interaction length L_2 . This double the MZI's modulation frequency as function of wavelength, reducing sigma'noise by a factor of 2.

$$S_3 = (\frac{1}{2}\sigma_{noise} + \sigma_{scan} + \sigma_T) \frac{1}{\frac{\partial \lambda_m}{\partial n_s}} \quad (35)$$

Equation 35 compared to equation 33 shows that increasing the interaction length L_2 only reducing the error caused by random noise. This is only useful when the random noise is dominant.

4.2 MEASUREMENT SETUP

In order to use an optical chip, a light source and optical detector are required. The light source used is a Vertical Cavity Surface Emitting Laser (VCSEL) (ULM850-B2-PL-So101U). A VCSEL is a small gain medium with a Bragg stack on either side of it. One of its properties is that the output wavelength is temperature dependent. This makes it possible to vary the output wavelength based on the temperature. However it is also possible to change the output wavelength by increasing the driving current, this will cause the gain medium's emission peaks to shift in wavelength based on the amount of current going through the VCSEL. The makes it possible to modulate the VCSEL a lot faster than when changing its temperature. But the drawback is that the output intensity also scales with the driving current, making

the output intensity to increase while sweeping the wavelength range. In our setup the VCSEL's driving current was modulated while keeping the external temperature constant. In this current setup the VCSEL's wavelength range limited by the power source is around 3500 pm centered between 850 nm and 860 nm, depending on the temperature. Figure 8 shows a diagram of whole measurement setup.

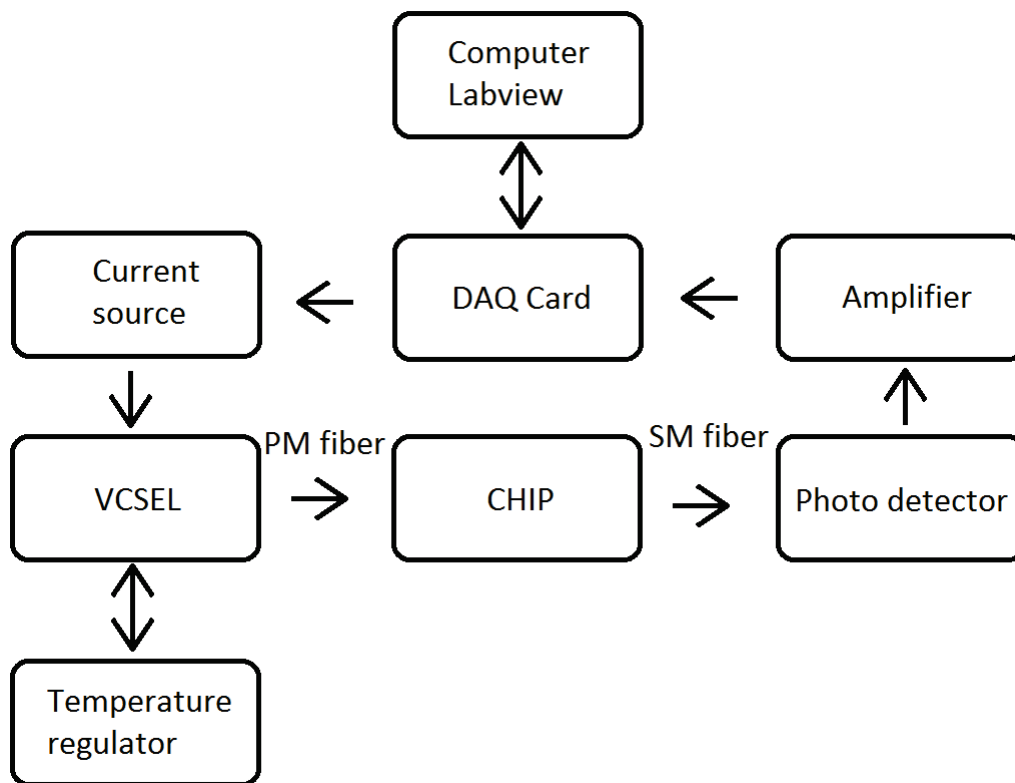


Figure 8: The DAQ card is sweeping the voltage of the current source's input over a certain range. The current source sends 1 mA output electrical current through the VCSEL per voltage of input. The VCSEL is stabilized in temperature to prevent the center wavelength from drifting. Light is coupled from the VCSEL to the optical chip using a polarization maintaining fiber. Light from the chip is coupled to an optical detector using a single mode fiber. The output signal from the optical detector is amplified and send to the DAQ card to be measured and send to the computer for processing.

In this diagram the output light of the VCSEL coupled into the optical chip with a polarization maintaining fiber. The optical chip itself is in this case either an optical chip with a MZI or MRR structure. Light coming out of the chip is coupled to a single mode fiber and detected by a photo detector. The photo detector (Thorlabs 125G-101HR-FC) is a component that generates a current based on the optical power. A component like this can be used to its full potential when its analog output is converted to a digital signal and send to a computer, for this a data acquisition (DAQ) card from Labview (USB-6353) is used. This DAQ card is also controlling the power source driving the VCSEL.

4.3 VCSEL CALIBRATION

The VCSEL is driven with an electrical current that sweeps from a minimum to a maximum current. When this current sweep is linear, then the output light does not have to be linear with inverse-wavelength. Instead a non-linear curve has to be used. This curve is obtained by measuring the modulation of a MZI and then normalizing it in intensity, so that a sine-like signal remains. Now the idea is to obtain a current curve so that the phase of the MZI signal is linear with data points or linear in time while sweeping the VCSEL. This phase from every data point is obtain by taking the inverse sine of the measured MZI modulation. After unwrapping the phase a curve is obtain that shows the phase as function of current. When swapping the axis, the final curve is obtained. This curve shows current as function of phase. The calibration gives is now obtain by resampling the curve to be equally spaced over the dependent axis.

If this calibration would not be linear, then the frequency components will become wider. The problem this can cause is that the measured phase obtain a systematical error as function of phase, which could change the responsivity. This error can be compensated for quite aggressively by calibrating every measurement, increasing the computational power required and adding a random error onto every measurement. Another approach would be by using a windowing function [2], this multiplies the input with an envelope that affects the Fourier transform. In case a windowing function can reduce the effect of this systematical error to become neglectable. But most windowing function also have drawbacks, the two most commons drawbacks are an small decrease in signal to noise and widening of the frequency components. This widening makes it harder to separate different frequency components if they are too close together, which is solved by designed the structure to have enough spectrum distance between the different components.

4.4 COMPARISON BASED ON EXPERIMENTAL MEASUREMENTS

In order to test the theory from previous section and to test if the temperature is homogeneous, we do a measurement on a MRR and a MZI. The design of the sensors used is shown in figure 9. The MRR has a physical length of $870 \mu m$ and is that same as the physical path-length difference of the MZI. The MZI also has two spirals with equal length of 6.4 mm. The sensors used in this measurement have no sensing windows. However if they would have a sensing window, then the MZI would have 7.3 times high responsivity than the MRR. If the total error of both the MRR and MZI would be the same, than the assumption of homogeneous is corrent. If the total error of the MZI is less than 7.3 times the total MRR error, than this MZI is more sensitive than the MRR.

In these measurement the wavelength spectrum shift was measured in time while heating the sensor up and letting it cool down again. Both these measurements also measure two equal sensors located around 1 mm from each other in parallel, this allows to subtract the the shifts from each other to obtain the total error. The figures 10 and 11 show the measured wavelength spectrum shifts of the sensors. These are two available sensor with a large difference in size, but nearly equal in output signal. The main difference is that the MRR has theoretically are larger error due to noise, but this is compensated by increases the light input power for the MRR to have equal effects of noise. For both the measurements it can be seen that both parallel sensors behave the same, but the larger size of the MZI makes it more sensitivity to non-homogeneous temperature fluctuations compared to the MRR. Figure 12 shows the

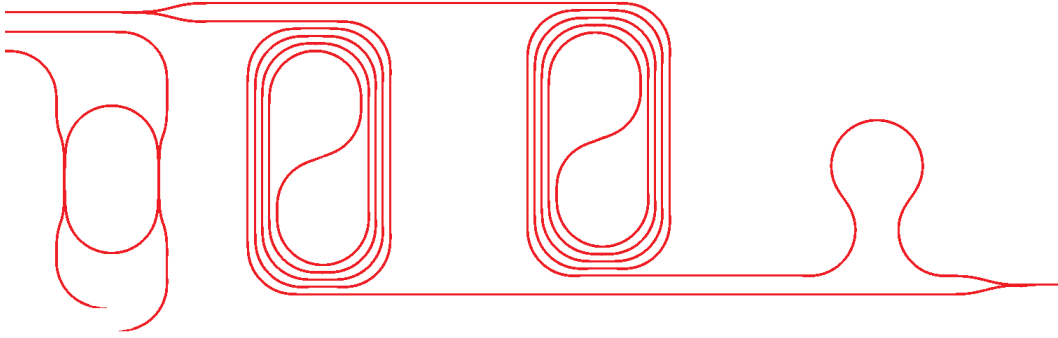


Figure 9: Two sensor structures are shown, a MRR and a MZI. Both these sensor have a physical path-length difference of $870 \mu\text{m}$. The spirals of the MZI have a physical length of around 6.4 mm . Both these structures are blind and have no sensing window, however the design has enough space to allow for a sensing window on a single or both spirals.

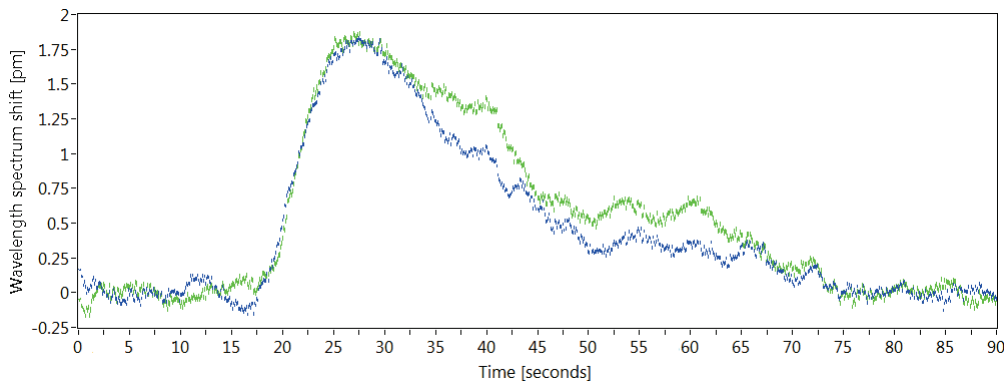


Figure 10: Resulting wavelength spectrum shift caused by heating up two MZIs by 0.5°C . The large size of these sensors cause for a large error due to temperature fluctuations than for the MRR.

differential signal between both the parallel sensors. The standard deviation averaged over the whole measured time interval for the MZI is 0.09 pm over 0.1 second and for the MRR is 0.03 pm over 0.1 second . In these measurements the standard deviation due to random noise was 0.015 pm over 0.1 second for both sensors. This error due to random noise is relatively high compared to typical measurements, this was due to low coupling between the VCSEL's light and the chip. The reason for this was to reduce back reflections towards the VCSEL. In a situation with optimal coupling this error contribution can easily be reduced by a factor of 10. So even if the responsivity of the MZI is 7.3 times higher it only results in a sensitivity that is 2.4 times larger than the MRR, due to the increased effect of temperature fluctuations on the larger sensor size. So these measurements show that the MZI is more sensitive than the MRR. It also shows that the assumption of the chip's temperature being homogeneous is not correct. So for a future sensor design it should be kept in mind that sensor size increases the effect of temperature fluctuations significantly, because the error due to random noise is low.

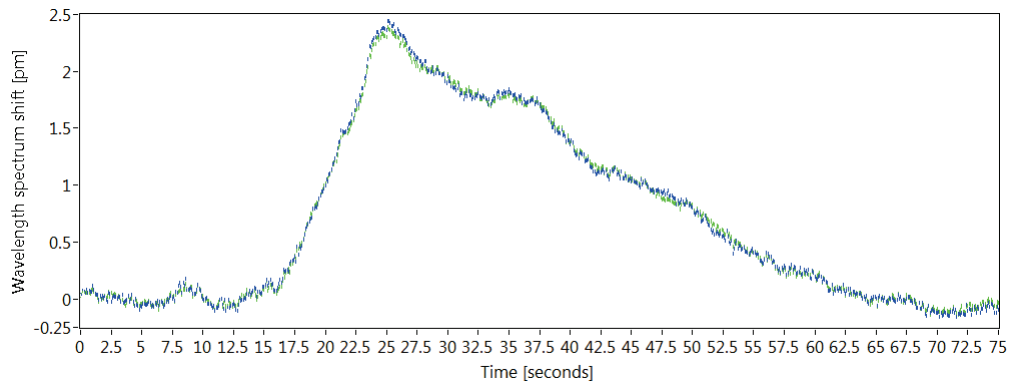


Figure 11: Resulting wavelength spectrum shift caused by heating up two MRRs by 0.7°C . The small size of these sensors cause for a small error due to temperature fluctuations.

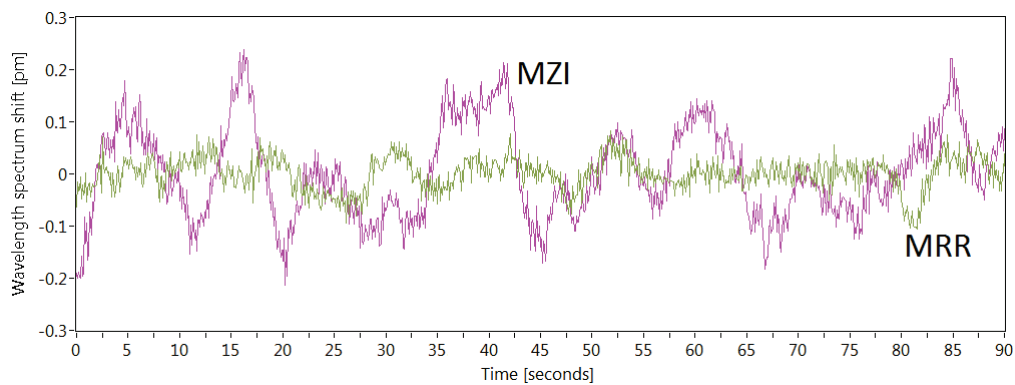


Figure 12: The wavelength spectrum shifts difference of both the parallel sensors. The total standard deviation of the MZI is 0.09 pm over 0.1 seconds averaged over the whole time interval, for the MRR this is 0.03 pm over 0.1 seconds . The standard deviation due to random noise is 0.015 pm over 0.1 seconds for both sensors

 MULTIPATH INTERFEROMETER

The wavelength spectrum of a Mach-Zehnder interferometer (MZI) has only a single intensity modulation frequency. This frequency is dependent on the path-length difference between the arms. When designing a structure, this length difference can easily take a preferred value. The Fourier transform (FT) allows to separate the different frequency components from a function. This makes it possible to use the Fourier transform to decompose a composite signal, consisting of signals from multiple different MZIs, into the individual signals, as long as all these MZIs have a different *FSR* (path-length difference). Sending multiple signals in the form of a single composite signal and then recovering the separate signals at the receiving end is called multiplexing. The advantage of multiplexing is that a single light source and photo detector can be used to measure multiple light interference signals at the same time. To our knowledge this had not yet been done for refractive index sensor. In this chapter a multipath interferometer is presented and multiplexing is demonstrated.

5.1 THEORY OF THE MULTIPATH INTERFEROMETER

When combining the physical output of multiple MZIs the interference between all light paths determine the output. These interferences should be taken into account when designing the structure. For instance when combining multiple MZIs, then the reference arms should not caused additional interference signals. This could be prevented by making all of them the same length. Instead it is also possible to have all the sensing arms share a single reference arm. So this interferometer becomes a multipath interferometer instead of a two-path interferometer. The additional interference signals between the sensing arms are not a problem as long as these signals do not affected the interference signal between sensing arms and reference. This is achieved by having a length difference ΔL between the sensing arms and a distance $(\frac{1}{2} + N)\Delta L$ between the reference arm and the sensing arms. Where N is an integer larger or equal to zero. To illustrated this, figure 13, shows a schematic representation of a multipath interferometer with 4 paths.

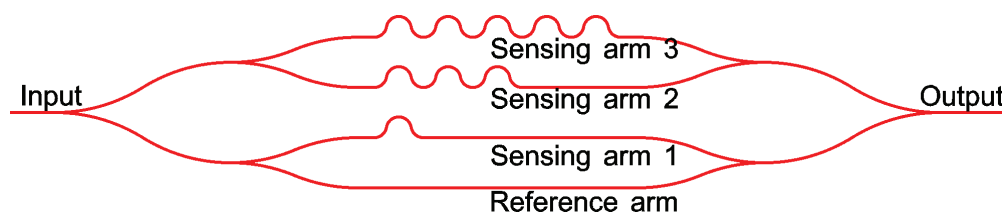


Figure 13: Schematic representation of a multipath interferometer with three sensing arms and one shared reference arm. At the output a composite signal of the interference between all paths is measured.

To get a better understanding of the output signal from the multipath interferometer, this structure is being calculated through for a one dimensional time independent case. The result from one dimensional gives a good overview of which parameters affect the outcome. For this calculation the electric field is defined as,

$$E = e^{ikz} \quad (36)$$

Where for this case z is the optical path-length with respect to the reference. For the reference arm this length is zero. For sensing arm 1 we choose this path-length difference to be $\frac{1}{2}\Delta L$. For sensing arm 2 we choose a relative length of $\frac{3}{2}\Delta L$ and sensing arm 3 a relative length of $\frac{5}{2}\Delta L$. The input amplitude is 1 [a.u.], which is split into the four amplitudes A , B , C and D , such that $A + B + C + D \equiv 1$.

$$E_r = Ae^{ik0} \quad (37)$$

$$E_{s1} = Be^{ik\frac{1}{2}\Delta L} \quad (38)$$

$$E_{s2} = Ce^{ik\frac{3}{2}\Delta L} \quad (39)$$

$$E_{s3} = DE_0e^{ik\frac{5}{2}\Delta L} \quad (40)$$

$$E_{out} = E_r + E_{s1} + E_{s2} + E_{s3} \quad (41)$$

A photo detector gives a measurable power output on the light intensity instead of electric field. In order to obtain the intensity, the electric field has to be multiplied with its complex conjugate.

$$I_{out} = E_{out}E_{out}^* = A^2 + B^2 + C^2 + D^2 + \frac{AB}{2}\cos(k\frac{1}{2}\Delta L) + \frac{AC}{2}\cos(k\frac{3}{2}\Delta L) + \frac{AD}{2}\cos(k\frac{5}{2}\Delta L) + \frac{BC+CD}{2}\cos(k\Delta L) + \frac{BD}{2}\cos(k2\Delta L) \quad (42)$$

This equation shows which physical arm contributes to which path-length difference. It shows that with these chosen path-length differences the interference between the reference and a sensing arm only has a contribution from a single sensing arm per path-length difference, which is essential for multiplexing. While the interference between the sensing arms occur at different path-length differences. So with these path-length differences it is possible to extract information from a single sensing arm without this information being affected by any other interference signal.

5.2 MEASUREMENTS

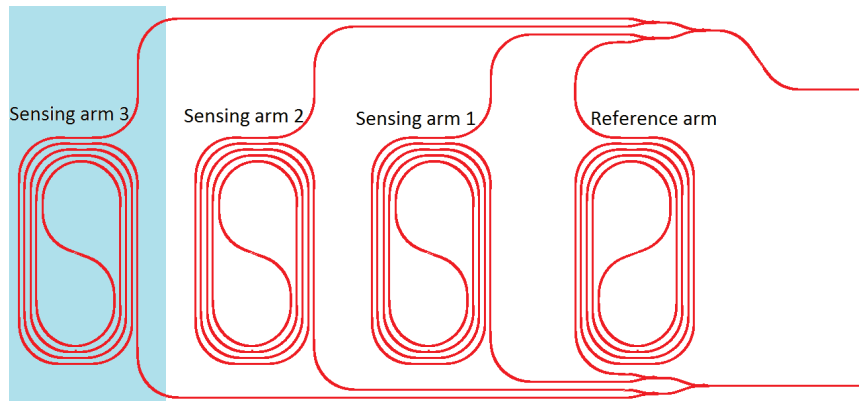


Figure 14: Mask design of the multipath interferometer with three sensing arms and one shared reference arm. Sensing arm 3 is inside the sensing window, represented as the colored rectangle at the left. The other arms are outside of the sensing window. At the output a composite signal of the interference signals between all paths is measured.

To test if multiplexing works the structure shown in figure 14 is used to measure refractive index changes. The path-length differences in this structure are designed as described in the previous section. This means that the distance between adjacent sensing arms is double the distance between the reference arm and the first sensing arm and is $2400 \mu m$. In this structure sensing arm 3 is placed inside the sensing window and sensing arms 1 and arm 2 are placed outside the sensing window. The reason for this is that when the response from the chip is different for different sensing arms, than it can be determined if composite signal can be decomposed in the individual signals. In the following measurements multiplexing is tested by determining if the sensing arm within the sensing window and the sensing arms outside the sensing window react as expected. For this two types of measurements are done, in the first measurement a refractive index change is applied only within the sensing window. For the second measurement the whole structure is heated up, this is done because a large difference in response to a temperature change is expected between the arms inside and outside the sensing window. A typical example of a measured wavelength spectrum from this structure is shown in figure 15, which shows that this signal is a composition of multiple modulation frequencies.

5.3 SENSING WINDOW REFRACTIVE INDEX CHANGE

This experiment uses the same setup as described in chapter 4. In order to gain a refractive index change in the sensing window we started with two cups of water with an initial volume of 40 ml each. One of these cups is used as reference, the other is used for measuring. In the measuring cup isopropyl alcohol (IPA) is added in steps of $20 \mu l$, which result in a refractive index change close to 2.6×10^{-4} for each step. In between these steps the sensor is placed from the reference cup into the measurement cup and then back into the reference cup. This was done to allow for stirring the content of the measurement cup without affecting the sensor and to obtain a homogeneous solution. The measured result is shown in figure 16.

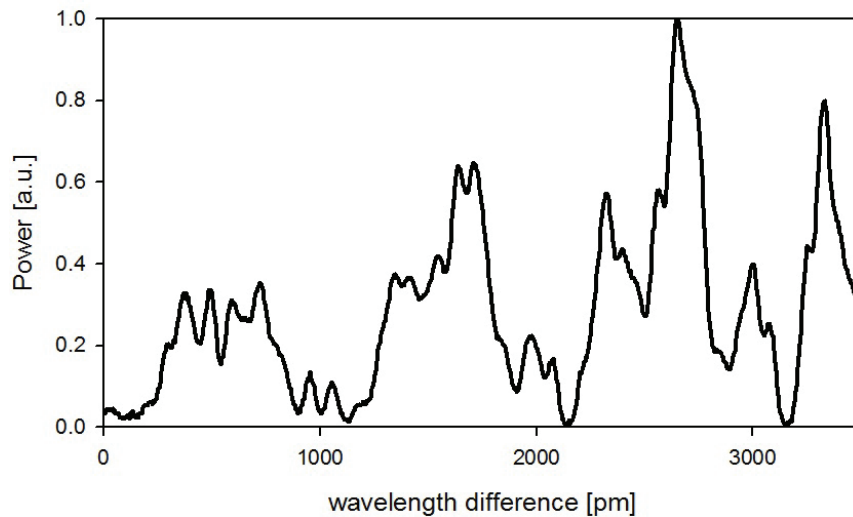


Figure 15: Measured wavelength spectrum of the multipath interferometer with interference from four arms. This shows that the signal is a composition of multiple modulation frequencies.

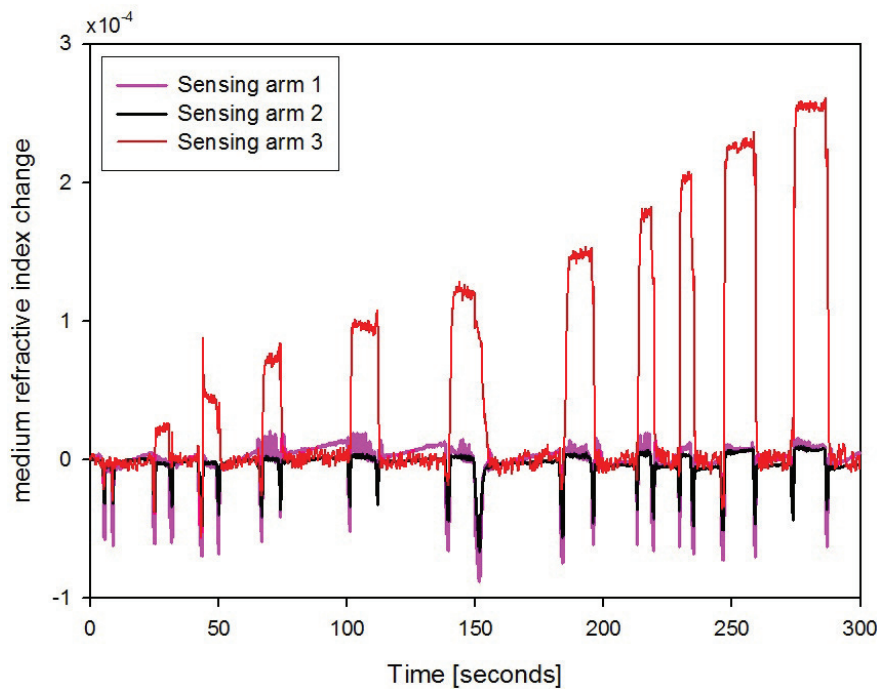


Figure 16: Measured wavelength shift of the multipath interferometer. The sensor is placed from the reference cup into the measuring cup and then back into the reference cup. The refractive index difference between the contents of these cups cause a wavelength spectrum shift in the signal from the sensing arm inside the sensing window, which has been translated to the refractive index change using the responsivity determined from figure 17. The arms outside the sensing window remain constant. The negative dips are caused when the sensor is traveling between the cups.

At start the chip was located in the reference cup, at 5 seconds the chip was placed in the measuring cup for a few seconds and then placed back into the reference cup. At this transition it

shows that the measured refractive index went down very shortly and then to the same level as the reference cup. These downwards spikes are produced when the chip is moved from one volume to the other. These downwards spikes do not affect the measured shift in a stable situation. For the first IPA step, 20 μl IPA is added to the measuring cup. The sensor is then placed from the reference cup into the measuring cup, kept there for a few seconds, then returned to the reference cup. This process is repeated for 10 of these IPA steps. The total IPA volume is a lot smaller than the initial water volume, so the wavelength shift to this refractive index change is assumed to be linear, as shown in figure 17.

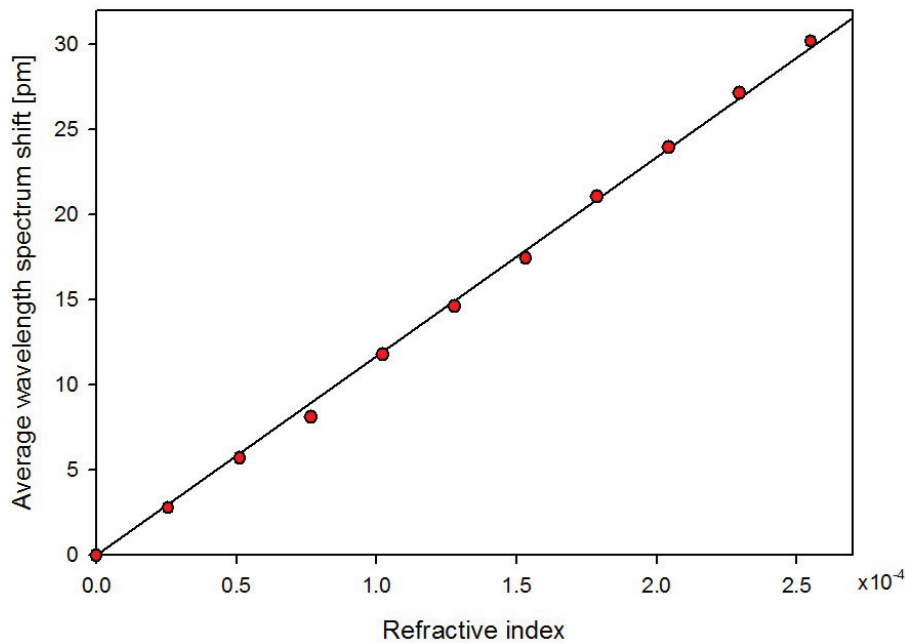


Figure 17: Measured wavelength shift of the multipath interferometer as function of the refractive index change applied to the sensing window. For each data point 20 μl of IPA was added to the initial solution of 40 ml water. This response is linear and the slope gives the responsivity of the sensor, which is 117 nm/RIU.

In figure 17 it can be seen that the wavelength shift is linear with refractive index change. This means that the sensor and data processing algorithm work as intended. The slope of the linear line gives the responsivity of this sensor, 117 nm/RIU. This responsivity is low for this sensor, but this is caused by a production error. In the production the sensing window was not etched open fully. A lower than expected responsivity was also noticed with the MRRs on that waver.

5.4 TEMPERATURE CHANGE

This second experiment starts with two initial cups of water. One at room temperature and the other above room temperature. The chip is placed in the water with room temperature and after that placed in the warmer water, this is repeated 3 times. The result is shown in figure 18.

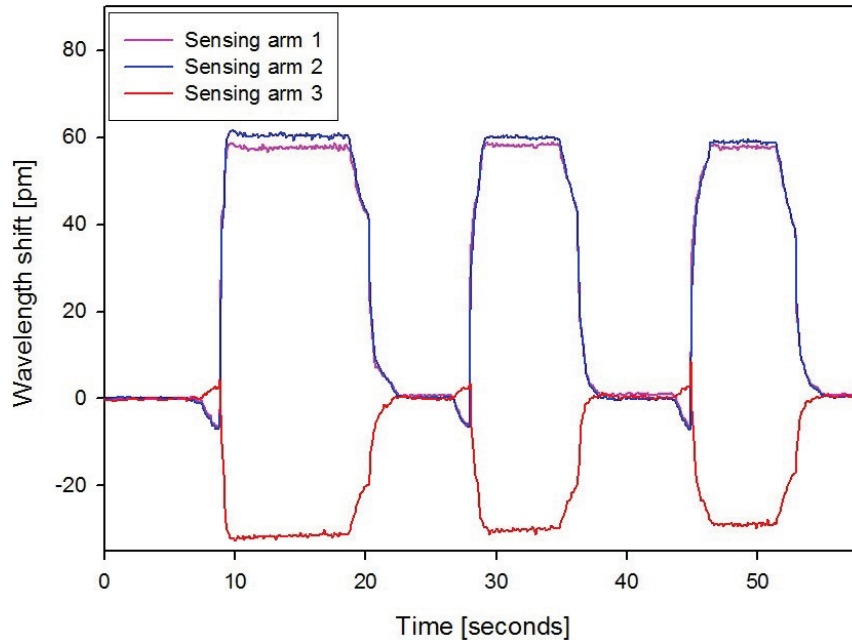


Figure 18: Measured wavelength shift of the multipath interferometer. The sensor is placed first in water at room temperature, then placed in warmer water and placed back into the water at room temperature. This was repeated three times.

This figure shows the wavelength shift of the signals between the sensing arms and the reference arm. When the temperature is increased than the signal of the arms outside of the sensing window get a positive wavelength shift, while the signal from the arm inside the sensing window gets a negative wavelength shift. This opposite sign in shift is in agreement with the temperature dependent properties of water. However in the ideal theoretical case, with no production error, the wavelength spectrum shift for the arm with sensing window should have been a lot larger.

5.5 CONCLUSION

The results from figures 16, 17 and 18 show that multiplexing is working. An advantage of this sensor is that the signal from multiple sensors can be measured at the same time using only a single detector. Another feature is that multiple sensing arms share a single reference arm, resulting in a small size compared to multiple separate sensors. The downside of this sensor is that it is a lot more sensitivity to systematical error. For instance fluctuations in the light coming from the VCSEL, this can be solved by calibration the system real time for every measurement.

 MORE ADVANCED USE MICRORING RESONATOR

6.1 ABSORPTION SENSOR

The MRR as refractive index sensor is not as good as the MZI. But the MRR has two measurable properties, the resonance shift and resonance width. In chapters 2 and 4 it was discussed how this resonance shift can be used. However, the resonance width was not yet taken into account.

The MRR's resonance width is affected by the phase and amplitude of the interfering light waves. The phase is determined by the optical path length of the ring and the small changes in refractive index do not cause the optical path length difference to change the resonance width. But the amplitude of the light waves is affected by the amount of propagation loss, where an increase in propagation loss widens that resonance width. This property is interesting, because it is unaffected by the (real part of the) refractive index and this property cannot be measured by the MZI with an easy method. So the MZI is better than the MRR at detecting refractive index change, but the MZI cannot measure small changes in absorption where the MRR can.

Chapter 3 described a method of translating the measured power as function wavelength to power as function of path length difference. For the MRR this returns a function that has a maximum power at path length difference equal to the round trip length and decreasing power for increasing number of round trip. We define the ratio q as the fraction of light that is not lost in the MRR per round trip. This ratio q can be determined by taking the power of round trip N and dividing it by the power of round trip $N - 1$. The loss per round trip due to propagation losses and out coupling is now given by $1 - q$.

With this ratio q it is also possible to easily determine the *FWHM* and finesse of the MRR. The *FWHM* is given by [5],

$$FWHM = \frac{2(1 - q) FSR}{\sqrt{q} 2\pi}. \quad (43)$$

The finesse is given by [5],

$$F = \frac{\pi\sqrt{q}}{1 - q}. \quad (44)$$

The ratio q is a combination of two loss contributions, this makes it very difficult to determine the absolute loss of one of these contributions. But it can be used to determine a change in absorption.

BIBLIOGRAPHY

- [1] Jean Baptiste Joseph Fourier. *Theorie Analytique de la Chaleur*. Firmin Didot Pere et Fils, Paris, 1822.
- [2] Fredric J. Harris. On the use of windows for harmonic analysis with the discrete fourier transform. *Proceedings of the IEEE*, 66:51–83, 1978.
- [3] IEEE. *IEEE 1057-2007 IEEE Standard for Digitizing Waveform Recorders*. 2008.
- [4] Luchansky MS and Bailey RC. High-q optical sensors for chemical and biological analysis. *Anal Chem.*, 84(2):793–821, 2012.
- [5] Katsunari Okamoto. *Fundamentals of optical waveguides*. Academic Press, San Diego, 2000.